communications earth & environment

ARTICLE

https://doi.org/10.1038/s43247-023-00780-y OPEN

Projected cross-shore changes in upwelling induced by offshore wind farm development along the California coast

Kaustubha Raghukumar[1✉], Timothy Nelson[1], Michael Jacox[2,3], Christopher Chartrand[4], Jerome Fiechter[5], Grace Chang[1], Lawrence Cheung[4] & Jesse Roberts[4]

In California offshore waters, sustained northwesterly winds have been identified as a key resource that can contribute substantially to renewable energy goals. However, the development of large-scale offshore wind farms can reduce the wind stress at the sea surface, which could affect wind-driven upwelling, nutrient delivery, and ecosystem dynamics. Here we examine changes to upwelling using atmospheric and ocean circulation numerical models together with a hypothetical upper bound buildout scenario of 877 turbines spread across three areas of interest. Wind speed changes are found to reduce upwelling on the inshore side of windfarms and increase upwelling on the offshore side. These changes, when expressed in terms of widely used metrics for upwelling volume transport and nutrient delivery, show that while the net upwelling in a wide coastal band changes relatively little, the spatial structure of upwelling within this coastal region can be shifted outside the bounds of natural variability.

[1] Integral Consulting Inc., Santa Cruz 95060 CA, USA. [2] NOAA Southwest Fisheries Science Center, Monterey 93940 CA, USA. [3] NOAA Physical Sciences Laboratory, Boulder 80305 CO, USA. [4] Sandia National Laboratories, Livermore 94550 CA, USA. [5] University of California Santa Cruz, Santa Cruz 95064 CA, USA. ✉email: kraghukumar@integral-corp.com

In California offshore waters, sustained northwesterly winds have been identified as a key energy resource, with the offshore wind resource potential estimated at 112 GW[1]. This resource could contribute substantially to California's renewable energy goals (Senate Bill 100) which require that at least 60% of California's electricity come from renewable sources by 2030, with a 2045 goal of powering all retail electricity sold in California and the state agency electricity needs with renewable and zero-carbon resources—those such as solar and wind energy that do not emit climate-altering greenhouse gases. The key advantage of offshore wind over its land-based counterpart is that the offshore wind resource is far more consistent, reliable, and energetic, with little of the topographic and small-scale variability typically observed over land. While turbines are limited to a theoretical maximum of ~59% of the energy from the wind that passes through the rotor area[2], floating offshore technologies are projected to operate at an average of 70% of their maximum power production capacity. The cost of producing that energy could decrease by as much as 53% by 2050[3]. California currently has planning goals of achieving 2–5 GW of electricity from offshore wind by 2030 and 25 GW by 2045. As of December 2022, commercial lease sales offshore of Humboldt and Morro Bay netted $757 million for the future rights to develop offshore wind farms in these areas. As promising as the offshore wind resource is, a lack of understanding of potential environmental effects is one current barrier to efficient permitting, development, and adoption of offshore wind that requires further investigation.

Wind-driven upwelling in the California Current is responsible for much of the primary productivity that sustains one of the richest ecosystems on the planet[4]. Wind-driven upwelling along the California coast is forced two ways (Fig. 1): first, northwesterly winds drive offshore Ekman transport near the coast, which produces coastal divergence and consequently, upwelling of cool, deep, nutrient-rich waters in a band adjacent to the coast whose width is approximately the local baroclinic Rossby radius of deformation (in the range of 10–20 km at these latitudes). Second, wind stress curl (horizontal gradients in the wind) drives divergent flow near the ocean's surface and consequently, upwelling (Ekman suction) that can extend 100–200 km farther offshore than that driven by coastal divergence[5,6]. In both cases, the occurrence of upwelling is characterized by the upward tilting of constant-density surfaces (isopycnals) towards the upwelling zone. Coastal upwelling has been found[5] to be more effective at introducing nutrients compared to local nutrient input from curl-driven upwelling, and productivity in the offshore region is predominantly the result of coastal upwelling together with offshore advection. Nonetheless, curl-driven upwelling has been suggested to support smaller plankton while coastal upwelling supports larger plankton, with potential implications for the success of different fish species[5].

An offshore wind farm project equal to an approximate lease block area of 20 km × 20 km is on the order of spatial scales at which rotational effects such as upwelling occur[7], the scale of which is closely connected to the local baroclinic Rossby radius of deformation and the scales over which a horizontal shear in wind speeds (wind stress curl) occur[8]. Since the development of offshore wind energy projects has the potential to not only reduce the wind stress at the sea surface, but also introduce wind stress curl, there is a possibility of local and/or regional implications on California coastal and curl-driven upwelling, nutrient delivery, and ecosystem dynamics. This study represents a first step towards gaining an understanding of the effects of offshore wind farms on upwelling ecosystems by characterizing changes in the physical circulation that can eventually inform a risk assessment and socioeconomic analysis. The main scientific questions that this study attempts to answer are:

- What are the effects of wind stress reductions by an offshore wind farm on upwelling circulation?
- What are the spatial and temporal patterns of changes in upwelling circulation?
- What are the effects of upwelling changes on nutrient delivery to the euphotic zone?

In light of the study questions above, the key finding of this study is that while wind farm wakes result in a local diminishment and enhancement in upwelling on either side of the wake, there is little net change in upwelling when integrated over a larger area that fully encompasses the wind energy areas of interest. However, changes in the spatial structure of upwelling due to wind turbines can be greater than the interannual changes that occur due to natural variability.

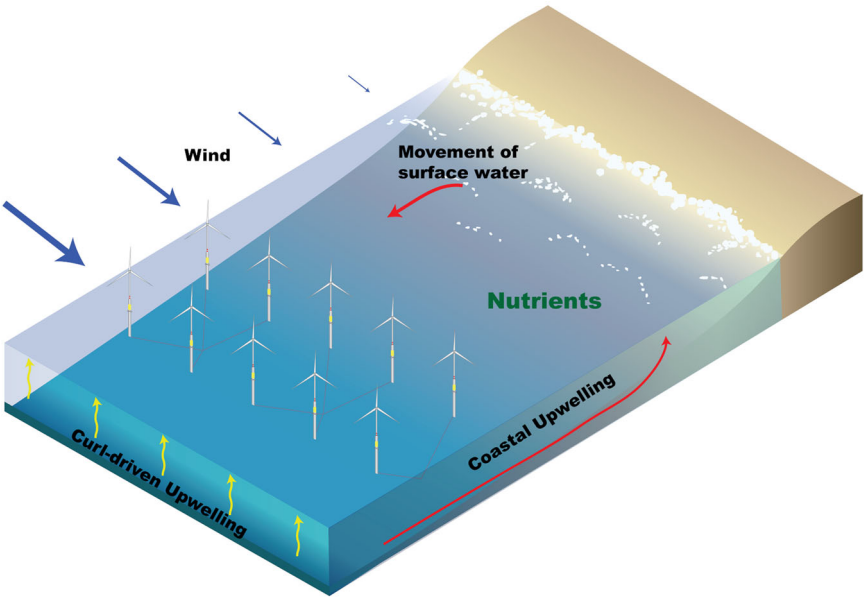

Fig. 1 Schematic of upwelling processes near an eastern ocean boundary. Coastal upwelling occurs in a narrow (10–20 km) coastal band and curl-driven upwelling over a larger offshore area. Figure adapted from Raghukumar et al. (2022)[16].

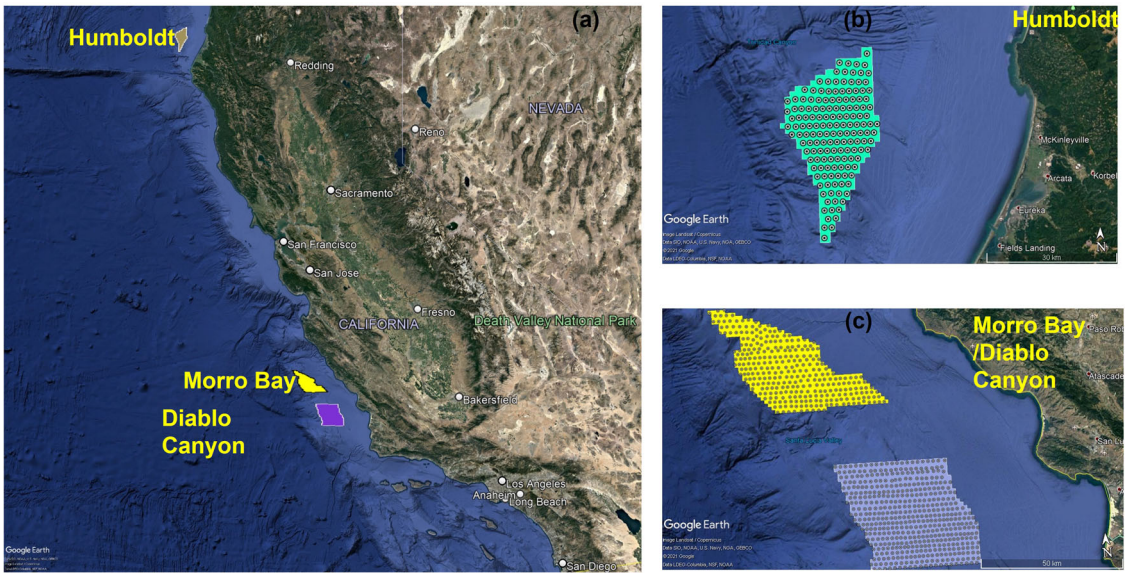

Fig. 2 Location of wind energy areas of interest along the California coast, and modeled layouts of turbines. a Wind areas of interest at Humboldt, Morro Bay, and Diablo Canyon, **b** modeled turbine layout at the Humboldt area of interest, and, **c** modeled turbine layout at the Morro Bay/Diablo Canyon wind energy area of interest. The circles within each area of interest represent the locations of modeled wind turbines. Note that since the start of this study, the Morro Bay wind energy area was reduced from 399 to 376 square miles. Also, as of December 2022, Morro Bay and Humboldt are recognized as California wind energy lease areas; Diablo Canyon area is not currently being considered for offshore wind planning. Maps Data: Google ©2021, Image Landsat/Copernicus, SIO, NOAA, U.S. Navy, NGA, GEBCO, LDEO-Columbia, NSF.

There are relatively few studies on the effects of large-scale offshore wind turbines on wind-driven upwelling. Wind stress reductions have been examined[9,10] for a large offshore wind farm in the North Sea and typical wind speeds 10 m above the sea surface were found to be reduced by up to 1 m/s (10%), with secondary effects on air temperature, relative humidity, and radiation. In response to changes in wind speeds, the formation of wind stress curl-driven upwelling in a large wind farm district was found to result in isopycnal displacement[8], indicative of changes to downwelling/upwelling, which increased as a function of wind farm lateral extent. Wind farm wakes are able to increase the magnitude of pycnocline displacements[11,12], and modulations in the pycnocline displacement can change the spatial–temporal patterns in coastal upwelling. Most recently[13], the presence of an upwelling/downwelling dipole was measured in the German Bight and characterized in terms of changes in mixed layer depth and potential energy. These studies focused on European wind farms, which are often in shallower water than is likely to be the case off the U.S. west coast and are not specifically located in a region such as the California Current System where contributions to wind-driven upwelling include both the wind stress curl and coastal components, both of which can potentially be affected by wind stress reductions.

Three California offshore areas of interest—Humboldt, Morro Bay, and Diablo Canyon—were originally recognized by the State of California and the Bureau of Ocean Energy Management (BOEM) [Docket No. BOEM-2018-0045] as regions with suitable offshore wind resources (Fig. 2)[1]. These sites in central and northern California are biologically and commercially important, providing habitat for multiple endangered species and supporting a commercial and recreational fishing economy valued at ~$22 billion[14].

Specific to California, two atmospheric models have been implemented in previous studies[15,16] for a hypothetical 10 × 10 km wind farm (8 MW turbines, 125 m hub height) offshore of Bodega Bay, California, and for a hypothetical buildout of 877 wind turbines (10 MW turbines, 128 m hub height) in 600–800 m deep waters offshore of Humboldt, Morro Bay, and Diablo Canyon. Both these studies found that wind speeds at 10 m height are reduced by approximately 5% (1 m/s), and at full build-out[16], wakes extended ~150 km downwind of the southern boundary of the wind energy areas of interest. While modeled wind speed changes were similar to those previously reported[9,10], the percentage reduction is smaller due to the higher wind speeds prevalent on the U.S. west coast and the fact that modeled wind turbine power production saturates above 12 m/s[17]. With the total length scale of wind speed reductions on the order of 250 km (since the Morro Bay and Diablo Canyon areas of interest span 100 km latitudinally), the changes reported[16] were on spatial scales large enough to influence upwelling off the U.S. west coast.

In this study, an atmosphere-ocean circulation model is applied to evaluate changes to coastal and curl-driven upwelling following the introduction of hypothetical wind turbine buildouts offshore at Humboldt, Morro Bay, and Diablo Canyon. Previously published wind fields in the presence of wind farms[16] provide the surface forcing fields that, in part, drive ocean circulation. A maximum possible turbine density is implemented in each of the modeled wind energy areas of interest. Since this density of turbines is not likely to be considered for an eventual buildout, the results presented can be considered to represent an upper bound on potential upwelling effects of California offshore wind. (Some caveats to this statement are: 1. There could be additional areas developed, which could increase the effects, and 2. The effects of the in-water turbine structures on mixing around the structures are not considered.)

Results

The atmosphere–ocean circulation model output is evaluated over a 25-year period spanning the years 1988–2012. A full buildout of turbines is modeled at the Humboldt, Morro Bay, and Diablo Canyon wind energy areas of interest. A one-way coupled modeling exercise was conducted, where atmospheric fields are first computed using the Weather Research and Forecasting model with the Wind Farm Parameterization (WRF-WFP).

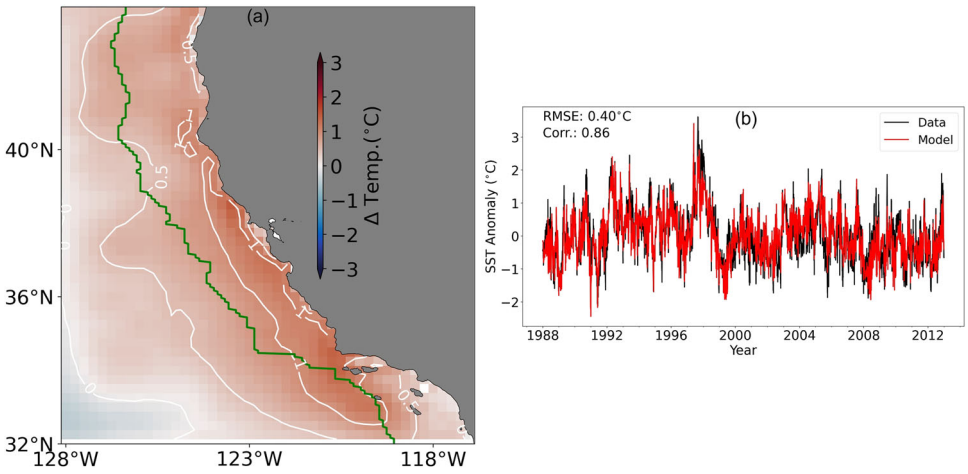

Fig. 3 Model-data validation of sea surface temperature. a Mean model-data bias in sea surface temperature (SST). White lines indicate 0.5 °C contours, while the green line indicates the boundary of the 0–200 km offshore zone used to compute **b** spatially averaged SST, relative to the seasonal mean, between 0 and 200 km offshore and 32–44°N, compared to those from the NOAA 1/4° OISST v2.1 product. RMSE = root mean square error and Corr = correlation coefficient.

Atmospheric fields near the ocean surface (winds, surface air temperature, relative humidity, precipitation, shortwave, and longwave radiation) are then used as forcing fields to the Regional Ocean Modeling System (ROMS), but no feedback of the ocean on the atmospheric lower boundary layer is modeled. Each model (atmosphere and ocean) has two nests, a 10 km-resolution outer nest, and a 3 km-resolution inner nest. Additional details on the specifics of each model are provided in the section "Methods".

Model validation. Model performance with respect to measurements was first established prior to evaluating the effects of wind turbines on upwelling circulation. Sea surface temperature (SST) data were obtained over the 1988–2012 period from the NOAA 1/4° Daily Optimum Interpolation Sea Surface Temperature (OISST version 2.1) product[18].

The model-data bias in SST is computed over the entire model domain of the 3 km-resolution model (Fig. 3a), while spatially averaged SST differences are computed along a zone that spans from the coast to 200 km offshore, between 32°N and 44°N, to focus on model performance within the coastal upwelling region (Fig. 3b). The seasonal cycle (i.e. the monthly mean climatology) is removed from the domain-averaged SST to focus on the model's ability to accurately capture interannual variability. The model was found to be biased and somewhat warm, with a root mean square error (RMSE; computed on the SST anomalies) of 0.4 °C. A good model-data correlation ($r^2 = 0.86$) is observed (Fig. 3), showing that the model has adequate skill in reproducing regional scale oceanographic processes that drive interannual variability, including warm surface waters during El Niño years (1997–1998) and cooler waters associated with La Niña years (1998–1999).

Model-data performance for salinity was also evaluated using data that spanned the years 1993–2012, along two transects, one in Monterey Bay (35–36.5°N) and other north of Point Conception (33–34.5°N), collected as part of the California Cooperative Oceanic Fisheries Investigations (CalCOFI). In general, it was found that the model reproduced the depth of the halocline but was biased salty between the surface and 150 m depth, and biased fresh between 150 and 300 m depth. The mean model-data bias of 0.17 psu was comparable to those previously reported[19], and acceptable given that salinity can be difficult for ocean models to reproduce because of the high uncertainty associated with external surface freshwater fluxes.

Vertical velocities. The effects of wind turbines on upwelling circulation are first examined by evaluating the different contributions of coastal and curl-driven upwelling (and the effects of wind turbines on each). This exercise is important due to the vastly different vertical velocities and spatial extents associated with each process, and therefore, the efficacy of each process in delivering nutrients to the euphotic zone. The contributions of coastal and curl-driven upwelling are often estimated by computing vertical velocities at the base of the mixed layer from the surface wind stress[5,20,21]. Typically, the vertical velocity at the base of the mixed layer associated with coastal upwelling is computed from the alongshore wind stress field, and the vertical velocity related to curl-driven upwelling (Ekman pumping) is calculated from the curl of the wind stress field. However, cross-shore gradients in the wind field often result in wind-stress curl within the coastal upwelling zone, making it difficult to separate the two effects. Here, vertical velocities are estimated at the base of the mixed layer associated with coastal and curl-driven upwelling by temporarily neglecting the cross-shore gradient in wind speeds in a narrow 10 km band next to the coast (i.e., upwelling inshore of 10 km is deemed coastal upwelling, and farther offshore is deemed curl-driven upwelling).

Using this approximation, vertical velocities are found to be generally about twice as strong for coastal upwelling (Fig. 4a) as for curl-driven upwelling (Fig. 4b) within the narrow 10 km coastal band. Vertical velocities at the base of the mixed layer near the coast are generally upwelling-favorable during the spring season (Fig. 4) and accentuated around headlands and topographic features such as Cape Mendocino, Point Arena, and Point Conception[22]. Curl-driven vertical velocities show both Ekman pumping and Ekman suction, depending on the polarity of the horizontal wind speed gradient. Differences in Ekman transport (Fig. 4c) due to wind energy extraction are primarily seen as a modest reduction in vertical velocity near Point Conception (34°N) and an even smaller reduction near Cape Mendocino. The nearshore side of the simulated wind farm shows a reduction in Ekman suction (Fig. 4d), which reinforces the reduction in coastal upwelling near Point Conception, while the offshore side of the simulated wind farm shows an enhancement in upwelling from Ekman suction.

Upwelling metrics. The model fields, evaluated in terms of metrics for upwelling volume transport (Coastal Upwelling Transport

Index [CUTI] and nutrient flux (Biologically Effective Upwelling Transport Index [BEUTI])[23]), exhibit similar seasonal and spatial variability, indicating that for the mean patterns, vertical nitrate flux (estimated by proxy from a temperature–nitrate relationship) closely tracks upwelling strength. While upwelling is strongest close to the coast (Fig. 5a), it can in some cases extend over 100 km offshore due to curl-driven effects[5,21].

The upwelling indices were therefore computed over a wide coastal band to capture any cross-shore differences in the effects of wind turbines on upwelling. Consistent with vertical velocity estimates calculated from the wind field (Fig. 4), the strongest upwelling transport is seen in a narrow band along the coast (Fig. 5a), with hotspots occurring near Cape Mendocino, Point Arena, and Point Conception. Comparing upwelling indices in the absence of turbines to the case with the wind field altered by turbines, a dipole-like pattern is observed in changes to upwelling (Fig. 5b). The sharp north–south boundary in the dipole structure is because the upwelling indices are calculated every 1° of latitude in the alongshore direction, consistent with operational upwelling indices published by the National Oceanic and Atmospheric Administration (NOAA)(https://oceanview.pfeg.noaa.gov/products/upwelling/intro). A reduction in upwelling transport is observed inshore of the simulated wind farms, accompanied by an increase in upwelling offshore of the wind farm areas. Changes are more pronounced at Morro Bay/Diablo Canyon than they are at Humboldt, likely due to the greater reduction in wind speeds and larger spatial extent of wind speed reductions in the larger Morro Bay/Diablo Canyon region. The changes in upwelling are primarily outside the 10 km coastal zone, which is usually the region of strongest upwelling[21].

Over the 25-year span of the model simulations, there is considerable natural variability in CUTI and BEUTI at 35°N (Fig. 6a, b, respectively), computed over a 100 km zone along a transect that runs through the Morro Bay/Diablo Canyon area, the region of greatest change in upwelling. Of particular note are years when upwelling was strongly inhibited by El Niño events (1992 and 1998). Depending on the year, CUTI and BEUTI can either be jointly suppressed (years 1991 and 1997) or enhanced (years 1999 and 2010) following the introduction of wind turbines. Further, in some years (1991, 1999) BEUTI can be enhanced even while CUTI is suppressed. The fact that nitrate flux (BEUTI) is decreased or enhanced more than upwelling transport (CUTI) indicates that the wind farm at 35°N changes not just upwelling strength, but also the subsurface temperatures of upwelled waters, and by proxy, the nitrate concentration of upwelled waters. Over the 100 km integration zone, changes in CUTI (BEUTI) were found to exceed the standard deviation of CUTI (BEUTI) just 1.43% (3.21%) of the time.

The magnitude of mean change in BEUTI and CUTI is sensitive to the offshore integration distance (Fig. 7c, d,

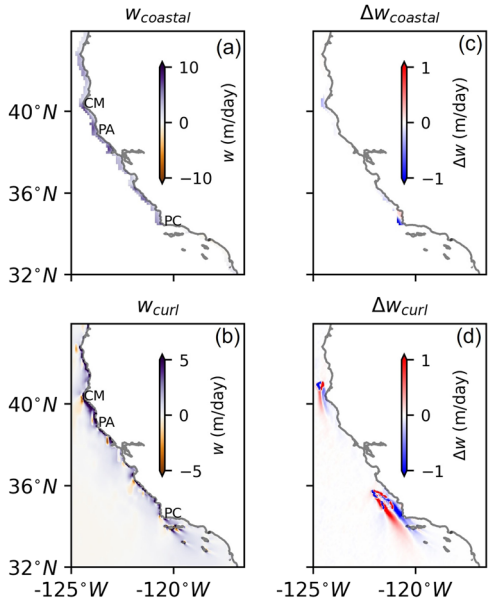

Fig. 4 Comparison of vertical velocities from coastal and curl-driven upwelling. Seasonally averaged estimates of **a** coastal and **b** curl-driven upwelling computed from wind fields during spring for the baseline case. Marked on the maps are Cape Mendocino (CM), Point Arena (PA), and Point Conception (PC). Differences in wind-driven vertical velocity estimates (turbines minus baseline) are shown for **c** coastal and **d** curl-driven upwelling.

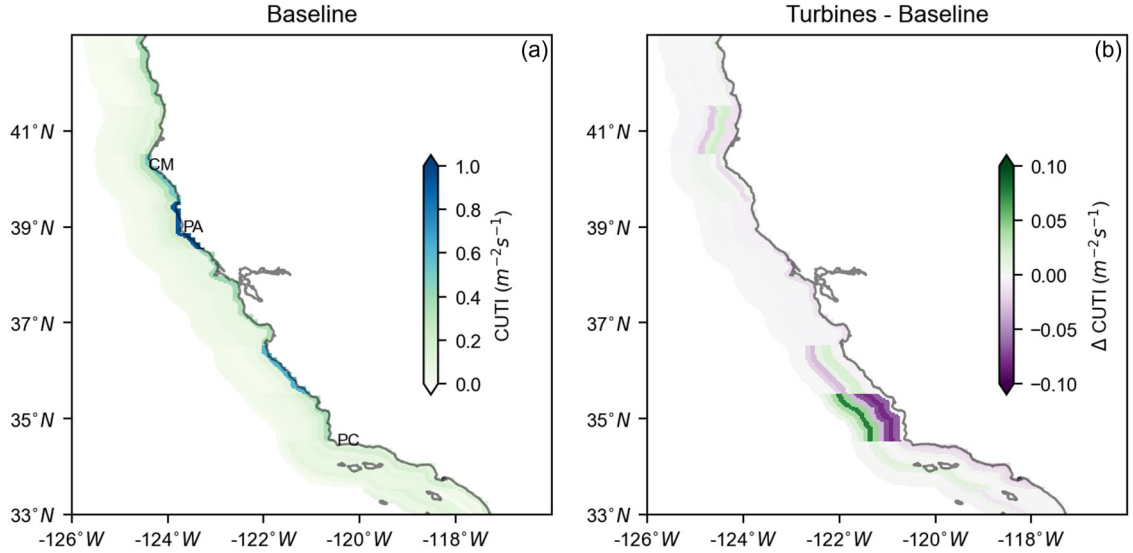

Fig. 5 Interannual mean of Coastal Upwelling Transport Index (indicating the strength of upwelling). Coastal Upwelling Transport Index (CUTI) for **a** baseline, and, **b** with turbines. CUTI shows a decrease in upwelling with the presence of turbines particularly nearshore (dark purple) and an increase offshore (green) at 35°N latitude. Marked on the maps are Cape Mendocino (CM), Point Arena (PA), and Point Conception (PC).

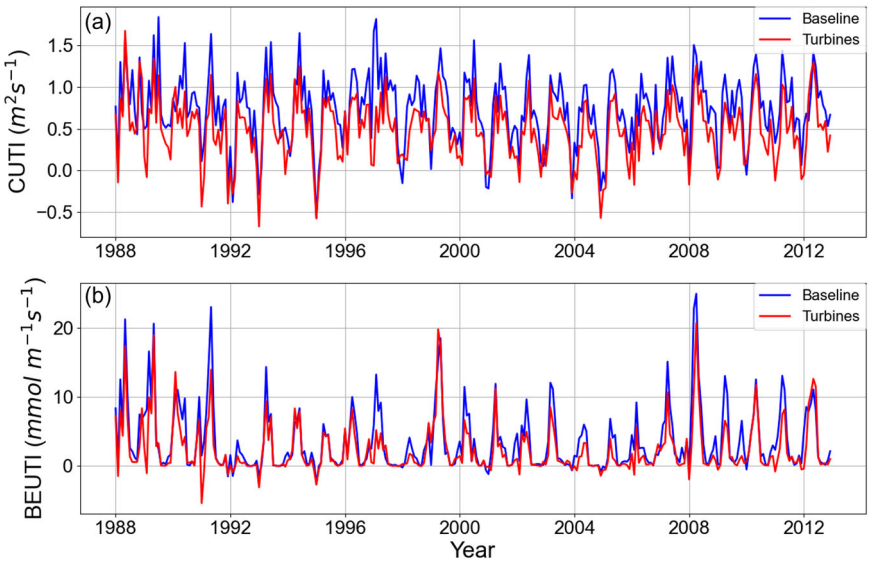

Fig. 6 Temporal evolution of upwelling metrics for volume transport and nutrient flux. a Coastal Upwelling Transport Index (CUTI) and **b** Biologically Effective Upwelling Transport Index (BEUTI) at 35°N, calculated over a 100 km zone.

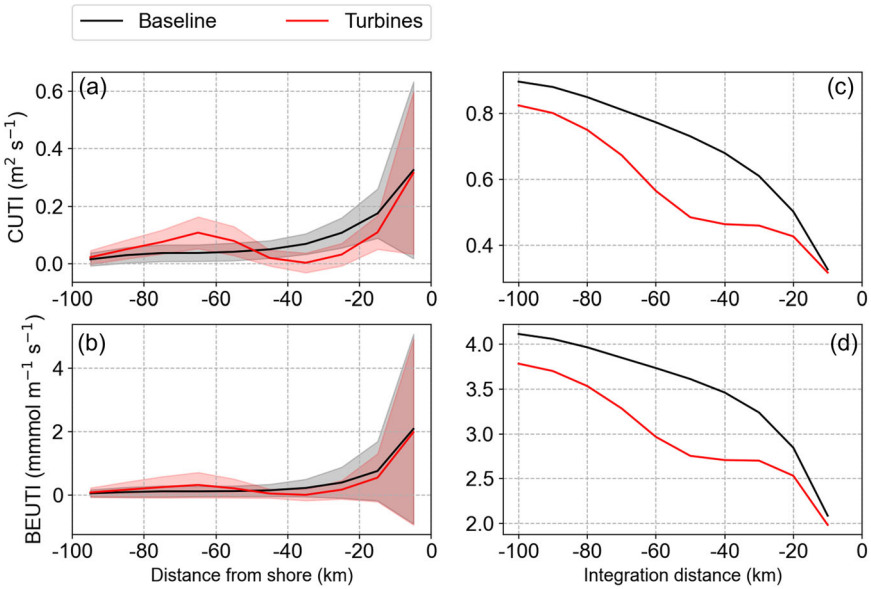

Fig. 7 Differences in upwelling metrics for volume transport and nutrient flux at 35°N. a Coastal Upwelling Transport Index (CUTI) and **b** Biologically Effective Upwelling Transport Index (BEUTI) as a function of distance from shore, calculated in 10 km bins, shown as bin-centered values. Shading indicates the interannual variability (i.e., standard deviation calculated across all years). Net upwelling at 35°N over increasingly wider swaths are shown in **c** CUTI, and, **d** BEUTI for various cross-shore integration distances, shown as values at the western edge of 10 km bins.

respectively) as upwelling decreases in an ~50 km nearshore zone are largely offset by increases in upwelling farther offshore. The maximum decrease in integrated upwelling transport and nutrient flux occurs 50 km from the coast (approximately in the center of the simulated wind farm) after which curl-driven upwelling increases help offset reductions in upwelling. Changes in CUTI and BEUTI are similar in that little to no change is observed in the 10 km zone adjacent to the coast, and the greatest reductions occur in the 10–50 km zone. The shading in Fig. 7 reflects the large interannual variability seen in CUTI and BEUTI (Fig. 6). However, in specific cross-shore regions (e.g., 20–40 and 60–80 km from shore), turbine-induced upwelling changes can fall well outside the natural variability (upper left, Fig. 7).

Surface and sub-surface temperatures. Baseline seasonal SSTs (Fig. 8, Winter: January–March, Spring: April–June, Summer: July–September, Fall: October–December), along with model-data differences (Fig. 3a), demonstrate that the model reproduces large scale temperature gradients such as the north-south gradient between the Oregon coast and Point Conception, and the warming of surface waters inside the Southern California Bight[19]. The model run in the absence of turbines produces upwelling patterns consistent with those previously documented for the U.S. west coast[19,24]. Upwelling is strongest in the spring/summer (Fig. 8b, c), with peak values occurring later in the year at higher latitudes. The strongest seasonal upwelling occurs in the vicinity of Cape Mendocino (38–40°N), with a secondary peak off central California, offshore of Morro Bay (~35°N). Changes to SST

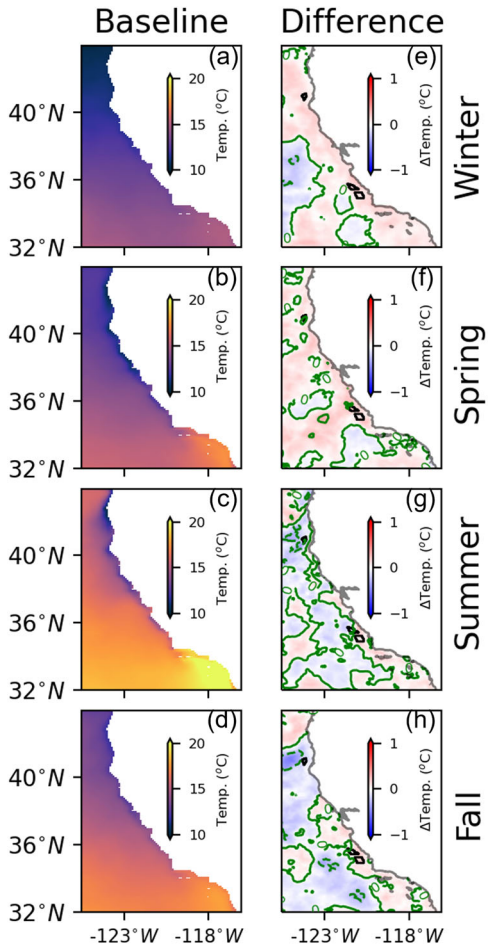

Fig. 8 Baseline and differences in sea surface temperature with turbines present. a–d Baseline seasonal sea surface temperature (SST), **e–h** seasonal differences in SST, turbines minus baseline. Wind energy areas of interest are demarcated by the black polygons.

following the introduction of wind farms are less than 0.5 °C, and much smaller than natural variability which can span 6–7 °C over seasonal and interannual cycles. Modeled changes primarily tend towards warmer temperatures in the winter (Fig. 8e, January through March), suggesting reduced upwelling of deeper, cooler waters to the surface as a result of the onset of upwelling in March. The warming pattern (relative to the case without turbines) continues to establish in the spring (Fig. 8f, April through June), particularly in the immediate vicinity of the Humboldt and Morro Bay/Diablo Canyon regions and is particularly noticeable along the offshore coastal upwelling jets[25] south of Cape Mendocino and north of Point Conception. Changes in SST are not particularly coherent in the summer (Fig. 8g, July through September) or fall (Fig. 8h, October through December), possibly due to the periodic relaxation and reversal of upwelling-favorable winds in these seasons[26,27], a seasonal increase in mesoscale activity along the offshore front of the upwelling jet and in the transition zone, and, internal variability in the California Current System eddy field which can lead to the offshore advection of coastal waters in the summer and fall[28]. Of note is that while wind speeds are only modified in the vicinity of these simulated wind energy areas of interest[16], the suggested changes in circulation throughout the model domain will require further exploration to understand.

Subsurface temperatures were examined due to their direct correlation to nutrient fluxes as computed by BEUTI (Fig. 9). Mean differences in subsurface temperatures over the 1988–2012 period along a transect at 35°N show a modest warming inshore of 50 km once simulated turbines are introduced in the environment, consistent with reduced upwelling in this zone. This warming is accompanied by the cooling of subsurface waters offshore of 50 km where increased local upwelling would lower temperatures and increase nutrient concentrations.

Discussion

The length and location of California's coastline along the eastern boundary of the Pacific Ocean result in a tremendous wind energy resource that is characterized by nearly year-round northwesterly winds. As promising as this wind field is as a source of offshore wind energy, it also supports a thriving marine ecosystem through wind-induced upwelling of cooler, nutrient-rich waters. The development of offshore wind in California will therefore need to consider the potential implications of offshore wind energy extraction on the California upwelling ecosystem. Here, a step towards addressing this concern is taken through the application of an atmosphere–ocean circulation model to evaluate the potential effects of offshore wind farms on upwelling. While this effort is focused on the California coast as a case study, the methods are applicable to coastal ecosystems where wind-driven upwelling plays a dominant role in nutrient delivery to the euphotic zone. The results of this study may, however, not be broadly applicable to other regions since there are site-specific nuances in upwelling circulation across regions such as differences in latitude, upwelling intensity/episodicity, aoelian transport, and the relative contributions of coastal and curl-driven upwelling[29].

The introduction of modeled wind turbines at three locations in the California Current alters the cross-shore structure of the wind stress gradient such that the mean nearshore–offshore gradient in wind stress is reduced (or reversed) on the nearshore side of the wind farm and enhanced on the offshore side of the wind farm, changing the pattern of wind stress curl and divergence associated with Ekman transport. Wind-stress curl has been suggested to have an important role in eastern boundary ecosystems[5], and the modifications to the wind-stress curl by the presence of an offshore wind farm will need further consideration in terms of impacts on primary and secondary production, and consequently on higher trophic levels.

Little change was observed at the Northern California (40°N) Humboldt wind energy area of interest in terms of indices for upwelling strength and nutrient flux. Further, no measurable change was observed within the highly productive 10 km coastal upwelling zone at either area of interest. However, around 35°N, the changes exhibit a dipole-like pattern[8,13], where a decrease in upwelling is seen on the inshore side of the wind farm and an increase in upwelling on the offshore side of the wind farm, in response to the polarity of the wind-stress curl. While the total upwelling strength, when calculated over a 100 km zone, shows little reduction, the pronounced change in the cross-shore structure of upwelling is in excess of natural variability. Specifically, at 35°N, upwelling strength 20–40 km offshore was reduced below what occurs naturally, while 50–70 km from shore upwelling strength was increased above the range of natural variability. Little change in net upwelling can be expected around wind farm wakes since the net change in wind stress curl can be small across the wind farm wakes. However, net changes in temperature (and nutrients) can be disproportional to net changes in upwelling due to distinct horizontal and vertical gradients exhibited by temperature and nutrient concentrations. The specific structure of the cross-shore wind stress gradient has been found to have a modulating effect on the strength of alongshore

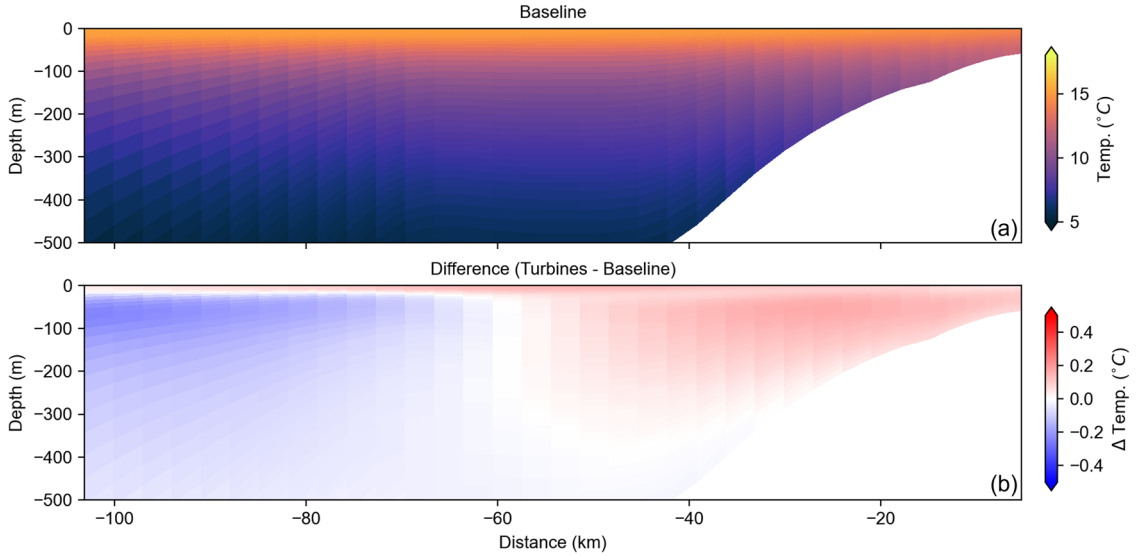

Fig. 9 Baseline and difference in subsurface temperatures with turbines present, at 35°N. a Baseline subsurface temperature over the 1988–2012 period, as a function of depth and distance to shore, and, **b** mean difference in subsurface temperatures, turbines minus baseline.

currents, eddy kinetic energy, and net primary productivity[30]. As a result of these often competing effects, there are periods when nutrient supply can remain stable or even increase despite reductions in upwelling strength. Some evidence of this decoupling can be seen in the results presented for specific years such as 1991 and 1999 when the nutrient flux (estimated by proxy from temperature) is enhanced even while upwelling strength is diminished.

While the results indicate a clear relationship between changes in wind speeds and the cross-shore structure of physical upwelling processes, no attempt is made to infer the ecosystem response based on changes to physical oceanographic processes. The accurate inference of ecosystem responses requires the specific computation of phytoplankton, zooplankton, and higher trophic level responses to physical driving factors[31,32], which is beyond the scope of this study. Further complicating the inference of ecosystem responses is the nonlinear relationship between the alongshore wind stress, nutrient fluxes, and primary productivity[33]. In terms of upwelling, peak productivity has been found to occur at moderate wind speeds that represent a trade-off between increased nutrient supply due to increasing equatorward winds and losses due to offshore advection at higher wind speeds. Other influencing factors include the duration of 'relaxation' events during the upwelling season and the width of the continental shelf[34]. Thus, while offshore wind farms cause a general reduction in wind stress in the lee of the wind turbines, the specific magnitudes of the resulting wind stress and the location of the wind farm will likely influence any reductions or increases in productivity.

It is worthwhile to consider the effects of offshore wind farms on modifications to upwelling circulation in the face of a rapidly changing climate. There has been a robust discussion on climate change impacts on upwelling circulation starting with Bakun[35], who suggested that global warming can result in more intense upwelling as a result of stronger alongshore winds induced by a greater land-sea air temperature difference and associated sea level pressure gradient. While positive trends in upwelling favorable winds have been observed off the California coast in recent decades[36], climate models project decreased upwelling-favorable winds along the California coast under continued anthropogenic forcing[37], and other factors also influence the dynamics of coastal upwelling. Surface-intensified ocean warming can increase stratification, thereby reducing the source depth of upwelled waters and inhibiting productivity[38], while basin-scale changes in circulation may alter the nutrient content of upwelling source waters, impacting productivity independent of local changes in winds or stratification[39]. The interplay of these sometimes competing effects will determine future changes in primary productivity off the California coast, and climate models do not agree on the expected sign of change[40]. The effect of wind farms should therefore be considered in the context of future change. For example, the reduction of upwelling in the 10–50 km cross-shore zone and the increase in upwelling farther offshore could reinforce or counteract climate change-induced upwelling changes. Similarly, the regions of reduced upwelling due to wind farms could act to reinforce the effects of increased stratification of the upper ocean, while the region of increased upwelling could help mitigate the effects of enhanced stratification. The complex interplay of these processes, therefore, deserves further consideration.

Also worth considering are advances in turbine technology that allows for 15 MW or higher-capacity turbines relative to the 10 MW turbines modeled here. The use of higher capacity turbines can result in a smaller or lower density build-out, or a more strategic placement of turbines within an area of interest, all of which can alter the magnitude and structure of the wind wake[41] and therefore influence changes in upwelling. The modeling of changes in upwelling due to both 15 MW turbines and other configurations of turbine buildouts is the subject of an ongoing study.

As with all modeling efforts, uncertainties are undoubtedly present. These include discretization effects (i.e. the finite resolution of the atmosphere and ocean model) that fail to resolve finer-scale processes and the effects of these on larger-scale processes. The use of a one-way coupled model (i.e., no ocean feedback on the lower atmospheric boundary layer) neglects well-known effects of upper ocean dynamics on the lower atmosphere[42,43] and vice-versa[44]. The use of a fully coupled model is, however, still an active area of research and not suitable for a study focused on a specific question such as this effort. The use of identical modeling approaches to evaluate the effects of wind farms on upwelling has the advantage of yielding comparative insights given that similar uncertainties exist in both the control run (no turbines) and in the modified state estimates

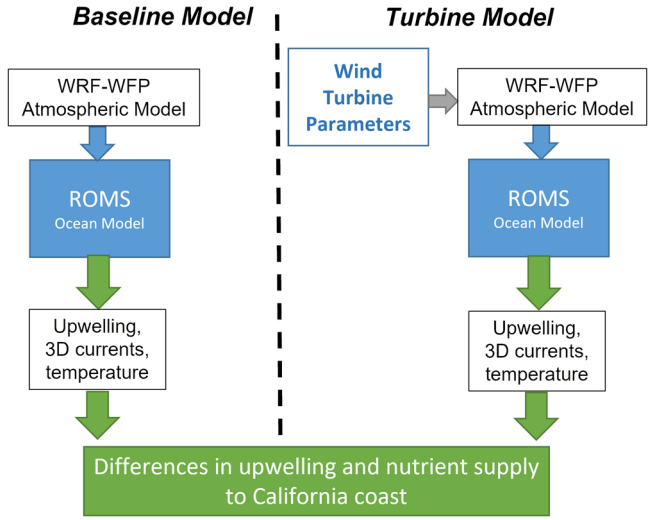

Fig. 10 Flowchart of atmosphere–ocean numerical modeling approach. Modeling approach to evaluate changes to upwelling following the introduction of an offshore wind farm.

(turbines present). Finally, these comparisons only account for the effect of the turbines on atmospheric circulation and the resulting changes in forcing to the ocean surface. They do not account for potential changes in ocean circulation due to the physical presence of wind turbines in the ocean and resulting wake-induced mixing around multiple wind turbine monopiles[45]. It is hoped that the results presented in this modeling study motivate a concerted effort to groundtruth or otherwise verify these results using alternate methods such as in situ or satellite measurements.

Conclusion

This study quantified the potential effects of upwelling ocean circulation induced by the presence of modeled wind turbines. The use of nested domains for the atmosphere and ocean circulation models allows for the resolution of processes on the scale of the wind energy areas of interest. The introduction of wind turbines primarily affects wind stress curl-driven upwelling, with little change observed in coastal upwelling. When cast in terms of metrics for upwelling strength and nutrient flux to the euphotic zone, a decrease in upwelling was seen on the nearshore side of the simulated wind farm, which was mostly offset by increases in upwelling on the offshore side of the wind farm. A pronounced cross-shore structure in changes to upwelling was observed, in excess of natural variability, while integrated changes indicated more modest changes in total upwelling. The consequences of these changes in physical upwelling structure on the ecosystem are currently unknown and could potentially form future areas of investigation that could also include an assessment of fisheries and socio-economic effects.

Methods

Advances in high-performance computing allow for the application of regional scale numerical circulation models to yield insights into the various driving forces and sensitivities of upwelling dynamics to these forcing mechanisms[19].

Atmospheric model. The modeling study is enabled using a high-resolution wind model, the Weather Research and Forecasting model with Wind Farm Parameterization (WRF–WFP[46]), which represents wind turbines as a momentum sink and turbulence source, using turbine parameters such as hub height, rotor diameter, power curve, and thrust coefficients to calculate the magnitude of the source and sink terms[47]. By allowing for wind farm parameterization within an established and validated operational weather model, WRF–WFP has been utilized in a number of studies to evaluate the effects of wind farms on mesoscale weather patterns[9,15,48]. The model accounts for turbine–turbine and wake–turbine interactions and thereby provides an accurate assessment of the wind field around a wind farm[49]. A WRF–WFP atmospheric circulation model was recently implemented[16] for the Eastern Pacific region, with a higher resolution nest that contains the continental shelf along the California coast. Simulated offshore wind turbines were placed within three wind energy areas of interest (Humboldt, Morro Bay, and Diablo Canyon). Each area of interest is roughly 40 × 40 km^2, and located ~30 km offshore. At the time of this writing, the Diablo Canyon area of interest is not actively under consideration, while the size and shape of the Morro Bay area have recently been modified (initially, Morro Bay 399 and now, Morro Bay 376). In this study, the Morro Bay 399 area boundary is used, along with the existing Humboldt and Diablo Canyon areas of interest. Specific details of the WRF–WFP model configuration were published in an earlier paper[16] and are summarized here for brevity. The resolution of the coarser resolution outer grid is 10 km and encompasses the region between 29.5°N to 48.5°N and 136°W to 110°W. The nested higher-resolution grid has a resolution of 3 km, and encompasses the region between 31.1°N to 45.25°N and, 130°W to 115°W. These wind fields (computed in the absence and presence of wind turbines) are used to force a regional ocean circulation model (Fig. 10), the Regional Ocean Modeling System (ROMS, see the section "Ocean circulation model") that also contains a higher resolution grid that encompasses the wind farms. While the finer resolution of 3 km has been found to result in turbine model convergence[50], the modeled 40 × 40 km^2 wind farm likely only resolved to 13–14 grid cells in each direction. This resolution, while limited, is sufficient in a Nyquist sense and implies that individual turbines are not resolved, but instead, the array acts as more of a continuum region applying the appropriate forces, in the aggregate, to the airflow.

Pressure and sea-surface temperature (SST) initial conditions and forcing fields were provided by the European Center for Medium-Range Weather Forecasts (ECMWF) Reanalysis v5[51]. The WRF model was initialized using these input conditions every 24 h and run for the subsequent 24 h. The first three hours for each day the model is run are considered the spin-up period and discarded. Previous studies[52] using mesoscale WRF models coupled to microscale wind farm simulations showed that while there were differences in the hub-height differences in turbulent kinetic energy and turbulent stress due to the initial conditions, these tended to vanish after a couple of hours, and resulting comparison of spectra showed promising agreement to measurements.

Nesting within this modeling system is one-way, i.e. there is flow from the coarse resolution to the finer resolution grid but not the opposite. This nesting allows for the computation of upwelling indices of relevance to primary production, and potential changes in these indices[23].

Turbine parameters. Turbine parameters (hub height of 128 m and a rotor diameter of 196 m, thrust and power coefficient curves) are taken from the 10 MW floating offshore turbine model described in[53] with a commercial operation date of 2022. Turbines are placed within each wind energy area of interest, assuming a full project build-out, as shown in Fig. 2. Water depths for the turbine locations range from 800 m to 2000 m, and the wind farms are located 35–50 km offshore. The locations of turbines within the Humboldt wind energy area of interest are identical to those previously reported[54], which consisted of 152 turbines spaced roughly 1.8 km apart (~9 turbine diameters, i.e. 9D spacing). A similar (9 turbine diameter) spacing was applied to the Morro Bay 399 and Diablo Canyon wind energy areas of interest, resulting in a total of 230 and 495 turbines in each Central Coast nominated wind energy area of interest, respectively, for a grand total of 877 turbines across the three areas.

Ocean circulation model. All ocean circulation modeling described in this study uses the ROMS[55]. ROMS is a free-surface, terrain-following, primitive equations ocean model widely used by the scientific community for a diverse range of applications[56–62].

The model consists of two domains: the outer domain (herein referred to as WC12) that spans from the middle of the Baja peninsula to the southern tip of Vancouver Island, and over 1000 km zonally, covering 30–48°N and 115.5–134°W, at 10 km resolution with 42 terrain-following vertical levels, while the inner nest (herein referred to as WC15) spans from 32–44°N and 116–128°W at a 3 km resolution, also with 42 terrain-following vertical levels. Surface forcing fields consists of WRF-WFP ([16]extended here to the period spanning years 1988–2012) horizontal wind speeds 10 m above the sea surface, air temperature and specific humidity 2 m above the sea surface, surface air pressure, precipitation, downward longwave radiation, and net shortwave radiation. The surface forcing fields for the WC12/WC15 domains consist of WRF fields from the outer/inner WRF domains, linearly interpolated onto the ROMS domains. Boundary and initial conditions for the WC12 model are derived from a data assimilative reanalysis of a previous version of the WC12 model[24]. The model was initialized starting in 1980, using the Simple Ocean Data Assimilation (SODA) analysis of the global upper ocean[63]. The 8-year spin-up period is sufficiently long to mitigate any dependence of the model solution on the initial conditions, typical of shorter-term predictions of chaotic

systems[64], and instead, the model solution is more sensitive to the forcing fields than a memory of the initial conditions[65].

Changes to upwelling circulation are evaluated using two model simulations spanning the years 1988–2012, one with turbines in the forcing fields, and one without turbines. This long simulation helps reduce statistical uncertainty and helps produce representative results on the effects of the specific turbine simulation scenario on upwelling circulation.

Both ROMS models (WC12 and WC15) have been utilized extensively in physical oceanographic and ecosystem studies of the California Current System, in addition to forming the basis of operational modeling at the Central California Ocean Observing System. The validated WC12 model[19] has been coupled to a lower-trophic level ecosystem models[31,32,66], and utilized in upwelling-specific studies[38] to look at upwelling variability using a historical analysis of the circulation of the California Current System and to examine canyon-driven nearshore upwelling and the resulting effects of larval transport[67]. It is recognized that the 3 km-resolution ocean model may not fully reproduce the ocean response, particularly with regard to sub-mesoscale features, and the influence of sub-mesoscale features on larger-scale upwelling[68]. However, there have been a wealth of studies that have shown that 3 km-resolution (and coarser) ocean models adequately reproduce both coastal and curl-driven upwelling. The ability of 20, 10, 5, and 3 km resolution US West Coast ROMS models to reproduce mesoscale circulation features has been evaluated[57], and convergence in the representation of coastal upwelling and mesoscale energetics appeared with the 5 km resolution model. A 1/3° (30 km) resolution model was found[69] to have resolved the coastal jet and mean features of the California Current System, including the magnitude and timing of upwelling. A 1/10° (10 km) resolution ROMS model of the US west coast adequately reproduced the timing and location of the spring upwelling along the US West Coast[19], when compared to surface altimeter maps of sea surface height. Further, the presence of 3 grid points in a 10 km swath can be considered as adequate in a Nyquist-sampling sense. The results of the study should therefore be interpreted as showing changes in upwelling features that are resolvable at 3 km, minus the possible influence of finer-scale features on the modeled upwelling phenomena.

The particular grouping of seasons (Fig. 8) was based on the understanding that April–May–June ("spring") has been defined[70] as the early upwelling season, July–August–September ("summer") the late upwelling/relaxation season, the three months prior to the upwelling season (January–February–March) is the "winter" or storm season, with October–November–December being the "fall" season.

Upwelling metrics. For 50 years, upwelling indices[71,72] have been used to monitor and understand coastal upwelling along the U.S. West Coast and its impacts on the marine ecosystem from phytoplankton to top predators. Initially, these indices were computed using coarse-resolution atmospheric pressure fields. More recent advances[23] have allowed more accurate quantification of upwelling and downwelling (i.e., the vertical transport into or out of the surface mixed layer) as well as nutrient fluxes associated with this transport. Specifically, two indices are routinely produced at NOAA's Southwest Fisheries Science Center: the Coastal Upwelling Transport Index (CUTI), which estimates vertical volume transport, and the Biologically Effective Upwelling Transport Index (BEUTI), which estimates vertical nitrate flux.

Here, CUTI and BEUTI indices are computed based on the high-resolution ocean and atmosphere model outputs described previously. Both indices are calculated in one-degree latitude bins along the U.S. west coast. The cross-shore extent of upwelling captured by the indices can be varied; typically a cross-shore integration distance of 75 km is used to encompass the productive nearshore region. Here, indices are also computed in 10 km cross-shore bins to better resolve the horizontal structure of upwelling changes within 100 km of the coast (wind energy areas of interest are centered ~45 km offshore). A detailed derivation of the upwelling indices is available in Jacox et al. 2018[23]. CUTI is the net horizontal transport in/out of a given latitudinal bin in the surface mixed layer, which must be balanced by vertical transport through the base of the surface mixed layer (i.e. upwelling or downwelling). CUTI is calculated as the sum of Ekman and geostrophic transports, each of which is integrated around the perimeter of the area of interest. Mathematically, CUTI is expressed as,

$$U^{\mathrm{Ek}} + U^{\mathrm{geo}} = \frac{\tau_0^y}{\rho f} - \frac{gD}{f}\frac{\partial \eta}{\partial y} \quad (1)$$

where τ_0^y is the northward wind stress, ρ the density at the base of the Ekman layer, f the Coriolis frequency, g the gravitational acceleration, η is the free surface height, and y the north–south axis. D is the depth of the Ekman layer, which is approximated by the mixed layer depth[73] with a 0.8 °C temperature threshold. Eq. (1) states that the near-surface cross-shore transport is the sum of the Ekman transport and the cross-shore geostrophic transport associated with an alongshore pressure gradient.

BEUTI, the vertical nitrate flux, is calculated by multiplying CUTI by the nitrate concentration at the base of the mixed layer. Since the ocean model does not explicitly represent nitrate, it is estimated from an empirical latitude–nitrate–temperature relationship that is very robust in the California Current System (capturing 95% of the observed nitrate variance[23]).

Data availability

The figure datasets generated for this study can be downloaded from the Sea Scientific Open Data Publication repository, https://www.seanoe.org/data/00829/94046/, https://doi.org/10.17882/94046.

Code availability

Codes used to generate main figures are available on request from the author (kraghukumar@integral-corp.com).

Received: 27 September 2022; Accepted: 28 March 2023;
Published online: 13 April 2023

References

1. Musial, W., Beiter, P., Tegen, S. & Smith, A. *Potential Offshore Wind Energy Areas in California: An Assessment of Locations, Technology, and Costs*. Technical report (National Renewable Energy Laboratory (NREL), Golden, CO, USA, 2016).
2. Gorban', A. N., Gorlov, A. M. & Silantyev, V. M. Limits of the turbine efficiency for free fluid flow. *J. Energy Resour. Technol.* **1**, 311–317 (2001).
3. Wiser, R. et al. Expert elicitation survey on future wind energy costs. *Nat Energy* **1**, 16135 (2016).
4. Xiu, P., Chai, F., Curchitser, E. N. & Castruccio, F. S. Future changes in coastal upwelling ecosystems with global warming: the case of the California Current System. *Sci. Rep.* **8**, 1–9 (2018).
5. Rykaczewski, R. R. & Checkley, D. M. Influence of ocean winds on the pelagic ecosystem in upwelling regions. *Proc. Natl Acad. Sci. USA* **105**, 1965–1970 (2008).
6. Checkley Jr, D. M. & Barth, J. A. Patterns and processes in the California Current System. *Prog. Oceanogr.* **83**, 49–64 (2009).
7. Szoeke, R. D. & Richman, J. On wind-driven mixed layers with strong horizontal gradients—a theory with application to coastal upwelling. *J. Phys. Oceanogr.* **14**, 364–377 (1984).
8. Broström, G. On the influence of large wind farms on the upper ocean circulation. *J. Mar. Syst.* **74**, 585–591 (2008).
9. Jiménez, P. A., Navarro, J., Palomares, A. M. & Dudhia, J. Mesoscale modeling of offshore wind turbine wakes at the wind farm resolving scale: a composite-based analysis with the Weather Research and Forecasting model over Horns Rev. *Wind Energy* **18**, 559–566 (2015).
10. Duin, M. Effect of wind farms at the North Sea on meteorological conditions in the Netherlands. Master's thesis (Wageningen University and Research, 2019).
11. Paskyabi, M. B. & Fer, I. Upper ocean response to large wind farm effect in the presence of surface gravity waves. *Energy Procedia* **24**, 245–254 (2012).
12. Paskyabi, M. B. Offshore wind farm wake effect on stratification and coastal upwelling. *Energy Procedia* **80**, 131–140 (2015).
13. Floeter, J., Pohlmann, T., Harmer, A. & Möllmann, C. Chasing the offshore wind farm wind-wake-induced upwelling/downwelling dipole. *Front. Mar. Sci.* **9**, https://doi.org/10.3389/fmars.2022.884943 (2022).
14. NMFS-F/SPO-187A, N.T.M. *Fisheries Economics of the United States 2016. Economics and Sociocultural Status and Trends Series*. Technical report (National Oceanic and Atmospheric Administration, National Marine Fisheries Service, 2018).
15. Huang, H.-Y. & Hall, A. D. *Preliminary Assessment Of Offshore Wind Development Impacts On Marine Atmospheric Environment: Final Project Report*. Technical report (UCLA Department of Atmospheric and Oceanic Sciences, 2015).
16. Raghukumar, K., Chartrand, C., Chang, G., Cheung, L. & Roberts, J. Effect of floating offshore wind turbines on atmospheric circulation in California. *Front. Energy Res.* **10**, 660 (2022).
17. Desmond, C., Murphy, J., Blonk, L. & Haans, W. Description of an 8 MW reference wind turbine. *J. Phys. Conf. Ser.* **753**, 092013 (2016).
18. Huang, B. et al. Assessment and intercomparison of NOAA daily optimum interpolation sea surface temperature (doisst) version 2.1. *J. Clim.* **34**, 7421–7441 (2021).
19. Veneziani, M., Edwards, C., Doyle, J. & Foley, D. A central California coastal ocean modeling study: 1. Forward model and the influence of realistic versus climatological forcing. *J. Geophys. Res. Oceans* **114**, https://doi.org/10.1029/2008JC004774 (2009).

20. Castelao, R. M. & Barth, J. A. Upwelling around Cabo Frio, Brazil: the importance of wind stress curl. *Geophys. Res. Lett.* **33**, https://doi.org/10.1029/2005GL025182 (2006).
21. Pickett, M. H. & Paduan, J. D. Ekman transport and pumping in the California Current based on the US Navy's high-resolution atmospheric model (COAMPS). *J. Geophys. Res. Oceans* **108**, https://doi.org/10.1029/2003JC001902 (2003).
22. Dorman, C. E., Mejia, J. F. & Koracin, D. Impact of US west coastline inhomogeneity and synoptic forcing on winds, wind stress, and wind stress curl during upwelling season. *J. Geophys. Res. Oceans* **118**, 4036–4051 (2013).
23. Jacox, M. G., Edwards, C. A., Hazen, E. L. & Bograd, S. J. Coastal upwelling revisited: Ekman, Bakun, and improved upwelling indices for the US West Coast. *J. Geophys. Res. Oceans* **123**, 7332–7350 (2018).
24. Neveu, E. et al. An historical analysis of the California Current circulation using ROMS 4D-Var: System configuration and diagnostics. *Ocean Model.* **99**, 133–151 (2016).
25. Lynn, R. J., Bograd, S. J., Chereskin, T. K. & Huyer, A. Seasonal renewal of the California Current: the spring transition off California. *J. Geophys. Res. Oceans* **108**, https://doi.org/10.1029/2003JC001787 (2003).
26. Huyer, A. Coastal upwelling in the California Current System. *Prog. Oceanogr.* **12**, 259–284 (1983).
27. Fewings, M. R., Washburn, L., Dorman, C. E., Gotschalk, C. & Lombardo, K. Synoptic forcing of wind relaxations at Pt. Conception, California. *J. Geophys. Res. Oceans* **121**, 5711–5730 (2016).
28. Strub, P. T. & James, C. Altimeter-derived variability of surface velocities in the California Current System: 2. Seasonal circulation and eddy statistics. *Deep Sea Res. Part II* **47**, 831–870 (2000).
29. Chavez, F. P. & Messié, M. A comparison of eastern boundary upwelling ecosystems. *Prog. Oceanogr.* **83**, 80–96 (2009).
30. Renault, L. et al. Partial decoupling of primary productivity from upwelling in the California Current System. *Nat. Geosci.* **9**, 505–508 (2016).
31. Goebel, N. L., Edwards, C. A., Zehr, J. P. & Follows, M. J. An emergent community ecosystem model applied to the California Current System. *J. Mar. Syst.* **83**, 221–241 (2010).
32. Fiechter, J., Edwards, C. A. & Moore, A. M. Wind, circulation, and topographic effects on alongshore phytoplankton variability in the California Current. *Geophys. Res. Lett.* **45**, 3238–3245 (2018).
33. Jacox, M. G., Hazen, E. L. & Bograd, S. J. Optimal environmental conditions and anomalous ecosystem responses: Constraining bottom-up controls of phytoplankton biomass in the California Current System. *Sci. Rep.* **6**, 1–12 (2016).
34. Botsford, L. W., Lawrence, C. A., Dever, E. P., Hastings, A. & Largier, J. Effects of variable winds on biological productivity on continental shelves in coastal upwelling systems. *Deep Sea Res. Part II* **53**, 3116–3140 (2006).
35. Bakun, A. Global climate change and intensification of coastal ocean upwelling. *Science* **247**, 198–201 (1990).
36. Sydeman, W. et al. Climate change and wind intensification in coastal upwelling ecosystems. *Science* **345**, 77–80 (2014).
37. Rykaczewski, R. R. et al. Poleward displacement of coastal upwelling-favorable winds in the ocean's eastern boundary currents through the 21st century. *Geophys. Res. Lett.* **42**, 6424–6431 (2015).
38. Jacox, M. G., Fiechter, J., Moore, A. M. & Edwards, C. A. ENSO and the California Current coastal upwelling response. *J. Geophys. Res. Oceans* **120**, 1691–1702 (2015).
39. Rykaczewski, R. R. & Dunne, J. P. Enhanced nutrient supply to the California Current Ecosystem with global warming and increased stratification in an earth system model. *Geophys. Res. Lett.* **37**, https://arxiv.org/abs/https://agupubs.onlinelibrary.wiley.com/doi/pdf/10.1029/2010GL045019. https://doi.org/10.1029/2010GL045019 (2010).
40. Bograd, S. J. et al. Climate change impacts on eastern boundary upwelling systems. *Annu. Rev. Mar. Sci.* **15**, https://doi.org/10.1146/annurev-marine-032122-021945 (2023).
41. Howland, M. F. et al. Collective wind farm operation based on a predictive model increases utility-scale energy production. *Nature Energy* **7**, 818–827 (2022).
42. Chalikov, D. & Belevich, M. Y. One-dimensional theory of the wave boundary layer. *Bound.-Layer Meteorol.* **63**, 65–96 (1993).
43. Krogsæter, O. & Reuder, J. Validation of boundary layer parameterization schemes in the Weather Research and Forecasting model under the aspect of offshore wind energy applications— Part I: Average wind speed and wind shear. *Wind Energy* **18**, 769–782 (2015).
44. Seo, H., Miller, A. J. & Norris, J. R. Eddy-wind interaction in the California Current System: dynamics and impacts. *J. Phys. Oceanogr.* **46**, 439–459 (2016).
45. Schultze, L., Merckelbach, L., Horstmann, J., Raasch, S. & Carpenter, J. Increased mixing and turbulence in the wake of offshore wind farm foundations. *J. Geophys. Res. Oceans* **125**, 2019–015858 (2020).
46. Fitch, A. C. et al. Local and mesoscale impacts of wind farms as parameterized in a mesoscale NWP model. *Mon. Weather Rev.* **140**, 3017–3038 (2012).
47. Lee, J. C. Y. & Lundquist, J. K. Evaluation of the wind farm parameterization in the Weather Research and Forecasting model (version 3.8.1) with meteorological and turbine power data. *Geosci. Model Dev.* **10**, 4229–4244 (2017).
48. Eriksson, O., Lindvall, J., Breton, S.-P. & Ivanell, S. Wake downstream of the Lillgrund wind farm-a comparison between LES using the actuator disc method and a Wind Farm Parametrization in WRF. J. Phys. Conf. Ser. **625**, 012028 (2015).
49. Churchfield, M. J., Lee, S., Michalakes, J. & Moriarty, P. J. A numerical study of the effects of atmospheric and wake turbulence on wind turbine dynamics. *J. Turbul.* **13**, 14 (2012)
50. Tomaszewski, J. M. & Lundquist, J. K. Simulated wind farm wake sensitivity to configuration choices in the Weather Research and Forecasting model version 3.8. 1. *Geosci. Model Dev.* **13**, 2645–2662 (2020).
51. Hersbach, H. et al. *ERA5 Hourly Data on Pressure Levels from 1979 to Present* (Copernicus Climate Change Service (C3S) Climate Data Store (CDS), 2018).
52. Haupt, S. E. et al. On bridging a modeling scale gap: mesoscale to microscale coupling for wind energy. *Bull. Am. Meteorol. Soc.* **100**, 2533–2550 (2019).
53. Beiter, P. et al. *The Cost of Floating Offshore Wind Energy in California Between 2019 and 2032*. Technical report (National Renewable Energy Lab. (NREL), Golden, CO, USA, 2020).
54. Severy, M. & Garcia, T. Description of study assumptions. In *California North Coast Offshore Wind Studies* (ed Severy, M. et al.) Humboldt (Schatz Energy Research Center, CA, 2020)
55. Shchepetkin, A. & McWilliams, J. *The Regional Ocean Modeling System: A Split-explicit, Free-surface, Topography-following-coordinate Oceanic Model* (Institute of Geophysics and Planetary Physics, University of California, Los Angeles, 2003)
56. Haidvogel, D. B. et al. Model evaluation experiments in the North Atlantic Basin: simulations in nonlinear terrain-following coordinates. *Dyn. Atmos. Oceans* **32**, 239–281 (2000).
57. Marchesiello, P., McWilliams, J. C. & Shchepetkin, A. Equilibrium structure and dynamics of the Current System. *J. Phys. Oceanogr.* **33**, 753–783 (2003).
58. Peliz, Á., Dubert, J., Haidvogel, D. B. & Le Cann, B. Generation and unstable evolution of a density-driven eastern poleward current: the Iberian poleward current. *J. Geophys. Res. Oceans* **108**, https://doi.org/10.1029/2002JC001443 (2003).
59. Di Lorenzo, E. Seasonal dynamics of the surface circulation in the Southern California Current System. *Deep Sea Res. Part II* **50**, 2371–2388 (2003).
60. Dinniman, M. S., Klinck, J. M. & Smith Jr, W. O. Cross-shelf exchange in a model of the Ross Sea circulation and biogeochemistry. *Deep Sea Res. Part II* **50**, 3103–3120 (2003).
61. Budgell, W. Numerical simulation of ice-ocean variability in the Barents Sea region. *Ocean Dyn.* **55**, 370–387 (2005).
62. Wilkin, J. L. et al. A regional ocean modeling system for the long-term ecosystem observatory. *J. Geophys. Res. Oceans* **110**, https://doi.org/10.1029/2003JC002218 (2005).
63. Carton, J. A., Chepurin, G. & Cao, X. A simple ocean data assimilation analysis of the global upper ocean 1950–95. Part ii: Results. *J. Phys. Oceanogr.* **30**, 311–326 (2000).
64. Branstator, G. & Teng, H. Two limits of initial-value decadal predictability in a CGCM. *J. Clim.* **23**, 6292–6311 (2010).
65. Corti, S. et al. Impact of initial conditions versus external forcing in decadal climate predictions: a sensitivity experiment. *J. Clim.* **28**, 4454–4470 (2015).
66. Raghukumar, K. et al. Impact of assimilating physical oceanographic data on modeled ecosystem dynamics in the California Current System. *Prog. Oceanogr.* **138**, 546–558 (2015).
67. Lowe, A. B. Modeling of coastal processes and Lagrangian transport around the Monterey Peninsula. Ph.D. thesis. (University of California Santa Cruz, 2020).
68. Capet, X., McWilliams, J. C., Molemaker, M. J. & Shchepetkin, A. F. Mesoscale to submesoscale transition in the California current system. Part I: Flow structure, eddy flux, and observational tests. *J. Phys. Oceanogr.* **38**, 29–43 (2008).
69. Broquet, G. et al. Application of 4d-variational data assimilation to the California Current System. *Dyn. Atmos. Oceans* **48**, 69–92 (2009).
70. García-Reyes, M. & Largier, J. L. Seasonality of coastal upwelling off central and northern California: new insights, including temporal and spatial variability. *J. Geophys. Res. Oceans* **117**, https://doi.org/10.1029/2011JC007629 (2012).
71. Bakun, A. *Coastal upwelling indices, west coast of North America, 1946–71. U.S.* Department of Commerce National Oceanic and Atmospheric Administration, NOAA Technical Report NMFS SSRF-671, pp. 103 (1973).
72. Bakun, A. *Daily and weekly upwelling indices, west coast of North America, 1967-1973 U.S.* NOAA Technical Report 16. Department of Commerce, National Oceanic and Atmospheric Administration, NOAA Technical Report NMFS SSRF-693, pp. 114 (1975).
73. Kara, A. B., Rochford, P. A. & Hurlburt, H. E. An optimal definition for ocean mixed layer depth. *J. Geophys. Res. Oceans* **105**, 16803–16821 (2000).

Acknowledgements

The team thanks the California Energy Commission and the Ocean Protection Council for supporting this work through cooperative agreement EPC-19-009 (CEC) and grant agreement C0210404 (OPC). Sandia National Laboratories is a multimission laboratory managed and operated by National Technology & Engineering Solutions of Sandia, LLC, a wholly-owned subsidiary of Honeywell International Inc., for the U.S. Department of Energy's National Nuclear Security Administration under contract DE-NA0003525.

We are deeply grateful to Mike Optis (formerly at the National Renewable Energy Laboratory) and Julie Lundquist (at the University of Colorado, Boulder), for their helpful insights in configuring and interpreting WRF–WFP results. Jerome Carman, Eli Wallach, and Arne Jacobson at Cal Poly Humboldt provided the turbine locations for the Humboldt wind energy area of interest. We have greatly benefited from input from our California Energy Commission Agreement Manager, David Stoms, and our project technical advisory committee: Genevra Harker-Klimeš, Jaime Jahncke, Fayçal Kessouri, Sharon Kramer, Chris Potter, Tyler Studds, and Susan Zaleski. We thank Andy Leising and Elliott Hazen from the National Oceanic and Atmospheric Administration, and Thomas Kilpatrick and Lisa Gilbane from the Bureau of Ocean Energy Management for comments on an earlier version of the manuscript.

Author contributions

K.R. and G.C. conceived this study; K.R., T.N., C.C., and M.J. conducted the modeling and analysis; G.C., L.C., J.F., and J.R. provided technical and programmatic oversight; K.R. drafted the manuscript and all authors contributed to manuscript revision, read, and approved the submitted version.

Competing interests

Authors K.R., T.N., and G.C. are employed by Integral Consulting Inc. The remaining authors declare that the research was conducted in the absence of any commercial or financial relationships that could be construed as potential competing interests.

Additional information

Supplementary information The online version contains supplementary material available at https://doi.org/10.1038/s43247-023-00780-y.

Correspondence and requests for materials should be addressed to Kaustubha Raghukumar.

Peer review information *Communications Earth & Environment* thanks Göran Broström and the other, anonymous, reviewer(s) for their contribution to the peer review of this work. Primary Handling Editors: Clare Davis. Peer reviewer reports are available.